# 4.71-Pbps-Throughput Multiband OXC Based on Space- and Wavelength-Granular Hybrid Switching


Takuma Kuno
*Department of Information and Communication Engineering*
*Nagoya University*
Furo-cho, Chikusa, Nagoya, 464-8601 Japan
kuno.takuma.g2@s.mail.nagoya-u.ac.jp

Takuro Ochiai
*Department of Information and Communication Engineering*
*Nagoya University*
Furo-cho, Chikusa, Nagoya, 464-8601 Japan
ochiai.takuro.e2@s.mail.nagoya-u.ac.jp

Reiji Higuchi
*Department of Information and Communication Engineering*
*Nagoya University*
Furo-cho, Chikusa, Nagoya, 464-8601 Japan
higuchi.reiji.s6@s.mail.nagoya-u.ac.jp

Kazato Satake
*Department of Information and Communication Engineering*
*Nagoya University*
Furo-cho, Chikusa, Nagoya, 464-8601 Japan
satake.kazato.z7@s.mail.nagoya-u.ac.jp

Kenji Cruzado
*Department of Information and Communication Engineering*
*Nagoya University*
Furo-cho, Chikusa, Nagoya, 464-8601 Japan
cruzado.kenji.p5@s.mail.nagoya-u.ac.jp

Ryuji Munakata
*Department of Information and Communication Engineering*
*Nagoya University*
Furo-cho, Chikusa, Nagoya, 464-8601 Japan
munakata.ryuji.m4@s.mail.nagoya-u.ac.jp

Yojiro Mori
*Department of Information and Communication Engineering*
*Nagoya University*
Furo-cho, Chikusa, Nagoya, 464-8601 Japan
mori@nuee.nagoya-u.ac.jp

Shih-Chun Lin
*Department of Electrical and Computer Engineering*
*North Carolina State University*
Raleigh, NC 27695 USA
slin23@ncsu.edu

Motoharu Matsuura
*Graduate School of Informatics and Engineering*
*University of Electro-Communications*
1-5-1 Chofugaoka, Chofu, Tokyo, 182-8585 Japan
m.matsuura@uec.ac.jp

Suresh Subramaniam
*Department of Electrical and Computer Engineering*
*The George Washington University*
800 22nd Street NW SEH 6570, Washington, DC 20052 USA
suresh@gwu.edu

Hiroshi Hasegawa
*Department of Information and Communication Engineering*
*Nagoya University*
Furo-cho, Chikusa, Nagoya, 464-8601 Japan
hasegawa@nuee.nagoya-u.ac.jp



2023 International Conference on Photonics in Switching and Computing (PSC) | 979-8-3503-2370-2/23/$31.00 ©2023 IEEE | DOI: 10.1109/PSC57974.2023.10297168



***Abstract*—We numerically and experimentally demonstrate a high-throughput and high-port-count OXC architecture based on space and wavelength-granular hybrid switching. Numerical simulations of several network topologies show the good routing performance of our OXC. Its transmission performance is evaluated through an experiment using C- and L-bands. The net OXC throughput of 4.17 Pbps and the OXC port count of 128 are demonstrated.**



***Keywords—optical cross-connect, space division multiplexing network, multiband network***


## I. Introduction

The capacity of photonic networks must be increased to accommodate the ever-increasing network traffic. Space division multiplexing (SDM) technologies utilizing multicore fibers (MCFs) or multiple single-core fibers (SCFs) are attractive candidates for expanding network capacity [1]. Another candidate, multiband transmission technologies, utilizes additional frequency resources such as L- and S- bands [2]. To introduce these technologies into photonic networks, high-port-count optical cross-connect (OXC) architecture that can bridge numerous cores and wavelengths is necessary. The currently deployed OXCs adopt wavelength selective switches (WSSs) configured in broadcast-and-select (B&S) or route-and-select (R&S) fashion [3]. In these architectures, the port count of WSSs must be greater than that of the OXC to attain directionless connectivity. As the port count of commercially available WSSs is limited to 48 [4], the viable OXC port count is less than 48. To expand the OXC port count with commercially available devices, multiple WSSs must be cascaded or parallelized; however, this demands a number of costly WSSs. Furthermore, the introduction of multiband transmission technologies increases WSS cost. Given this background, optical matrix switches are gathering attention because numerous ports can be implemented in a cost-effective way [5]. The barrier to introducing optical matrix switches into the OXC lies in their low routing performance due to the lack of wavelength selectivity. To resolve this problem, we have proposed an OXC architecture based on space- and wavelength-granular hybrid switching, where high-port-count matrix switches and low-port-count WSSs are exploited to attain practical routing flexibility [6]. Although this architecture still has a routing constraint due to contention, network simulations have already shown that the routing performance virtually matches that of the ideal OXC. A proof-of-concept transmission experiment with a 16×16 OXC prototype with 300.8 Tbps throughput was reported in Optical Fiber Communication Conference 2023 [6].

This paper demonstrates, for multiband transmission systems, a 128×128 OXC prototype based on space- and wavelength-granular hybrid switching. Numerical simulations of several network topologies show the good routing performance of the proposed OXC. In the experiment, we measure the bit-error ratio (BER) of 184-wavelength 32 Gbaud dual-polarization 16-ary quadrature amplitude modulation (DP-16QAM) signals on a 50 GHz grid in the C- and L-bands. The net OXC throughput reaches 4.71 Pbps (= 128×184×200 Gbps). According to the authors' knowledge, this is the largest throughput reported so far.

## II. Optical Cross-Connect Architectures

Figs. 1(a) and 1(b) show a conventional $N \times N$ OXC employing the B&S and the R&S architectures [3],


This work was partly supported by NICT, NSF, and JSPS/KAKENHI (JP22J23852).

respectively, where use in S-, C-, and L-band systems is assumed. The $N\times N$ OXC based on the B&S architecture comprises $N$ $1\times(N+1)$ splitters and $N$ $(N+1)\times 1$ WSSs for each band. On the other hand, the R&S configuration consists of $N$ $1\times(N+1)$ WSSs and $N$ $(N+1)\times 1$ WSSs for each band. Here, S-, C-, and L-band WSSs are used in parallel and bridged by WDM splitters/couplers. If the OXC port count is expanded over ~10, excessive power loss is yielded by the $1\times(N+1)$ splitters in the B&S OXC. If the OXC port count is over 48, WSSs must be cascaded or parallelized to create a virtual high-port-count WSS. Unfortunately, to achieve high OXC port counts, this architecture needs too many costly WSSs. Fig. 2 shows the proposed OXC, where use in S-, C-, and L-band systems is assumed. The $N\times N$ OXC consists of $N$ WDM splitters, $3N$ optical amplifiers, $N$ $3\times(B+1)$ splitters, $B$ $N\times N$ matrix switches, $N$ $1\times 3$ splitters, $3N$ $(B+1)\times 1$ WSSs, $3N$ optical amplifiers, and $N$ WDM couplers. The routing procedure is as follows: First, optical paths from incoming fibers are partitioned into S-, C-, and L-bands by WDM splitters; After power compensation by optical amplifiers, optical signals are distributed to matrix switches by the splitter, where one port of the splitter is used as a drop port; After that, the signals are delivered to optical couplers by matrix switches; Finally, signals are delivered to WSSs, where one input port of the WSS is used for adding signals from local transmitters.

The key attribute of this OXC architecture is its scalability. As shown in Section 3, design parameter $B$ in Fig. 2 can be 3. Consequently, a high-port-count OXC can be realized by combining $1\times 4$ WSSs and high-port-count matrix switches; both of which are commercially available. Moreover, the matrix switches are shared by signals in multiple bands; as a result, the cost-effectiveness of the proposed OXC is highlighted in multi-band systems.

## III. Network Simulations

We confirmed the routing performance of the OXC through numerical simulations. The examined network topologies are a $4\times 4$ regular-mesh network, TMN23, and US LATA, as summarized in Table I. The available bandwidth of each fiber is 9.6 THz, operating under the presumption of C- and L-band transmission, with 768 12.5 GHz frequency slots. The path establishment requests are generated to yield source and destination nodes with random and uniform distribution. The average number of optical paths between each node pair is parametrized as traffic intensity. Three types of optical paths are considered, namely, 100 Gbps, 400 Gbps, and 1 Tbps, which necessitates 4, 7, and 15 frequency slots, respectively. Each optical path type has equivalent path occurrence probability. For the purpose of comparison, the routing performance of the all-WSS-based OXC is used as the baseline architecture though this architecture is impractical in terms of hardware cost. This OXC can route arbitrary input signals to arbitrary output ports except where prevented by wavelength contention on a fiber. Each plot shows the average value of 20 calculations.

Fig. 3 plots the number of necessary fibers versus traffic intensity, where the number of fibers is normalized by the results obtained by the non-restricted OXC. The penalty of the proposed OXC is large in the small traffic intensity area. This penalty originates from the fact that the number of accessible adjacent nodes becomes smaller due to the shortage of fibers connected to nodes. The penalty in routing performance is reduced by increasing $B$. The penalty in terms of fiber increment in the high-traffic intensity areas is less than 3% for all examined network topologies when $B$ is 3 and larger. Thus, $B$ should be set to 3 to balance routing performance against hardware cost.

## IV. Experiments

We conducted transmission experiments using C- and L-bands and confirmed the feasibility of our OXC architecture; Adding S-band is straightforward as shown in Fig. 2. Fig. 4 shows the experimental setup, where a part of the $128\times 128$ OXC was implemented. At the transmitter, a continuous wave (CW) generated from a tunable laser was formed to a

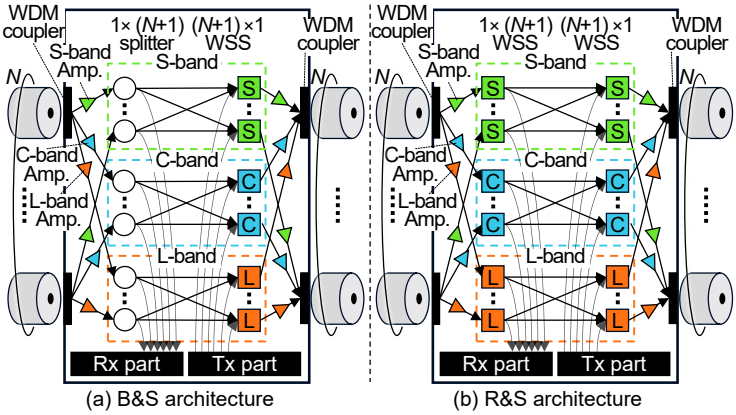


Fig. 1. Conventional OXC architectures.

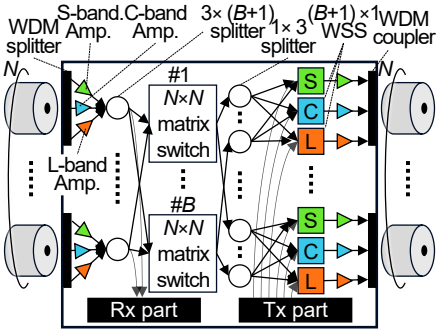


Fig. 2. Proposed OXC architecture.

TABLE I. Tested Network Topologies

| | | | | |
|---|---|---|---|---|
| Network topology | | 4×4 regular-mesh | TMN23 [7] | US LATA [8] |
| # of nodes | | 16 | 23 | 11 |
| # of links | | 24 | 43 | 23 |
| Node deg. | Max. | 4 | 5 | 8 |
| | Min. | 2 | 3 | 2 |
| | Ave. | 3 | 3.74 | 4.18 |

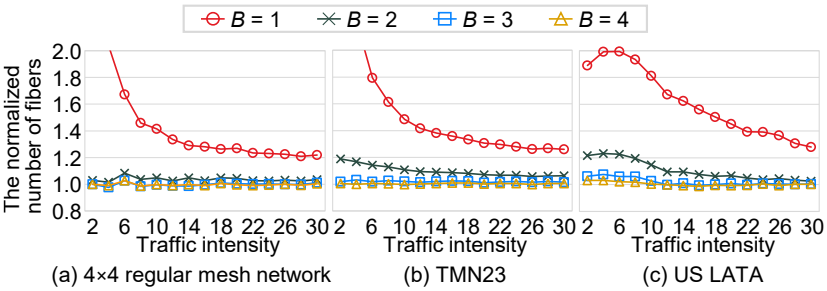


Fig. 3. The normalized number of necessary fibers against traffic intensity.

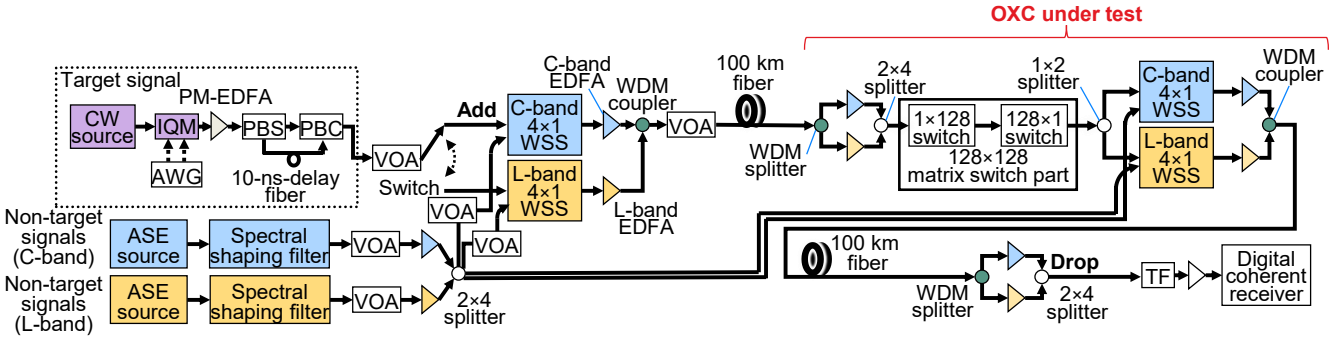


Fig. 4. Experimental setup.

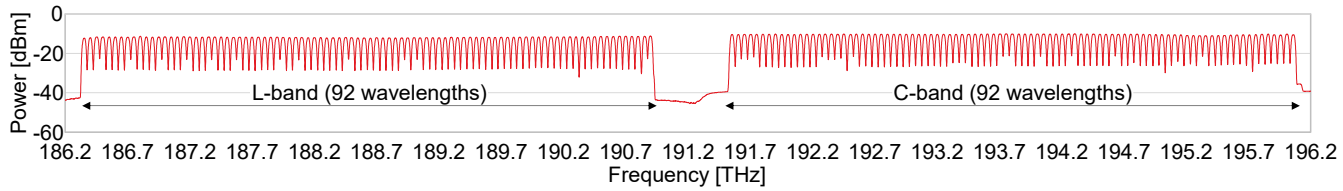


Fig. 5. Signal spectra before transmission.

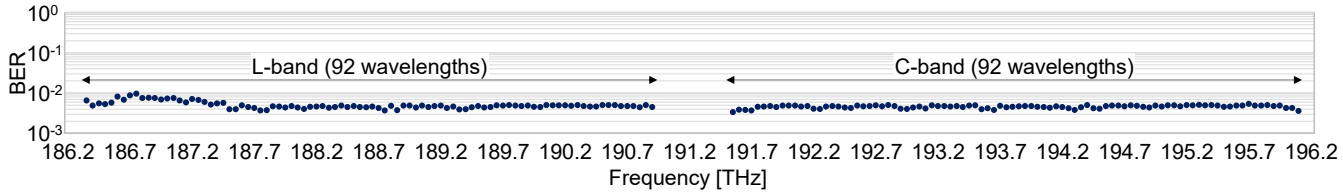


Fig. 6. Experimentally measured BERs.

32 Gbaud DP-16QAM signal by an IQ modulator (IQM) driven by an arbitrary-waveform generator (AWG). After power amplification by the polarization-maintaining (PM) EDFA, polarization-division multiplexing (PDM) was conducted by a PDM emulator consisting of a polarization-beam splitter (PBS), a delay fiber, and a polarization-beam combiner (PBC). This yielded a 32 Gbaud DP-16QAM signal. As non-target signals, 184-wavelength signals aligned on 50 GHz grid in C- and L-bands were emulated by amplified spontaneous emission (ASE) sources and spectral shaping filters. The 2×4 optical splitter distributed non-target signals to four 4×1 WSSs. After the power of the target signal was adjusted by a variable optical attenuator (VOA), the target signal and the non-target signals were combined by a 4×1 WSS. After power amplification by EDFAs, signals in C- and L-bands were combined by a WDM coupler, and overall power was optimized by a VOA. Fig. 5 shows the signal spectra, where the signal powers were adjusted by the spectral shaping filters to within ±0.9 dB. The signals were launched into a 100 km optical fiber whose dispersion coefficient, loss coefficient, and nonlinearity coefficient were 16.5 ps/nm/km, 0.19 dB/km, and 1.5 /W/km, respectively. After that, signals were input to the OXC under the test. The 128×128 OXC consisted of a WDM splitter, a 2×4 coupler/splitter, a part of a 128×128 matrix switch, a 1×2 optical splitter, 4×1 WSSs for C- and L-bands, EDFAs for C- and L-bands, and a WDM coupler. Considering the simulation results shown in Fig. 3, design parameter $B$ was set to 3. Therefore, the 2×4 splitter and the 4×1 WSSs were used in the OXC. The OXC loss was 21 dB in total. Note that the target signal from the 1×2 splitter was extracted by a 4×1 WSS, while the non-target signals coming from the 2×4 splitter were extracted by the WSSs. Therefore, the target signal suffered spectrum narrowing with OXC traversal. After OXC traversal, the signals were launched to a 100 km optical fiber. After passing through a WDM splitter and EDFAs, the signal was dropped by the 2×4 coupler/splitter. The target signal was then extracted by a wavelength tunable filter and processed by a digital coherent receiver.

Fig. 6 plots the BER of the 184 wavelength signals. We observed flat BERs of the signals over 187.7 THz. The quality of the signals under 187.7 THz was slightly degraded due to the noise figure of EDFAs and photosensitivity of the photodiodes in the receiver. However, all wavelengths attained acceptable BERs. The total OXC throughput of this prototype reached 4.71 Pbps.

## V. Conclusion

This paper demonstrated a 4.71-Pbps-throughput 128×128 OXC for future SDM and multiband networks. Its feasibility was successfully confirmed through network simulations and transmission experiments. This architecture is fully extensible because matrix switches with over 500 ports are already commercially available.

## References


[1] B. J. Puttnam et al., Optica, vol. 8, no. 9, pp. 1186-1203, 2021.

[2] N. Deng et al., J. Lightw. Technol., vol. 40, no. 11, pp. 3385-3394, 2022.

[3] S. L. Woodward et al., Chapter 15 in Optical Fiber Telecommunications VIB, Academic Press, 2013.

[4] Finisar, "Flexgrid twin 1x48 wavelength selective switch," https://www.globenewswire.com/newsrelease/2021/10/04/2307857/0/en/Finisar-AustraliaReleases-the-World-s-First-Flexgrid-Twin-1x48-Wavelength-Selective-Switch.html, accessed on 9 July, 2023.

[5] A. C. Jatoba-Neto et al., J. Opt. Commun. Netw., vol. 10, no. 12, pp. 991-1004, 2018.

[6] R. Munakata et al., OFC, paper M4G.8, 2023.

[7] T. Tachibana et al., IEICE Trans. Commun., vol. E106.B, no. 4, pp.296-306, 2023.

[8] S. Kim and S. Lumetta, J. Opt. Commun. Netw., vol. 1, no. 4, pp. 154-163, 2002.